Delayed deformation of confinement buildings: 30-years in-situ measured data and prediction with the next-generation Eurocode-2

Abudushalamu Aili, Jean-michel Torrenti, Francis Barre, Ludovic Caba

Delayed deformation of confinement buildings: 30-years in-situ measured data and prediction with the next-generation Eurocode-2

Abudushalamu Aili[1], Jean-Michel Torrenti[2,3], Francis Barre[4], Ludovic Caba[5]

[1]Graduate school of Environmental Studies, Nagoya University, Nagoya, Japan

[2]Université Gustave Eiffel, Champs-sur-Marne, France

[3]ESITC Paris, Arcueil, France

[4]Géodynamique et Structure, Bagneux, France

[5]EDF DIPNN DT, Lyon, France

Correspondence: jean-michel.torrenti@univ-eiffel.fr

Abstract

Biaxially prestressed large concrete structures of the confinement building in nuclear power plants should meet the safety requirement for the extension of the service time. Long-term delayed strains of concrete are one of the key factors determining the safety factor in these structures. This article presents 30-year long in-situ measurement results of strain evolution of confinement buildings in four different nuclear power plants. The delayed strains are predicted at a material level using the next-generation Eurocode 2, and the influence of temperature as proposed by the fib model code 2010, making use of delayed strain characteristics of the corresponding concrete from a previous study. We found that the default law given in Eurocode underestimates the delayed strain. However, with provided possibility of adjusting the shrinkage and creep laws, the prediction results fit with a good accuracy the in-situ measurement.

Keywords: creep, shrinkage, in-situ measurement, long-term, Eurocode,

Highlights

- Delayed strains of confinement buildings were measured for more than 30 years.
- Delayed strains predicted by the default laws given in Eurocode 2 are lower here than the measurement results of the used concretes.
- With the adjustment based on laboratory experiments, delayed strains of concrete are reasonably well predicted.

1 Introduction

The emergent climate crises due to global warming require the construction sector to reduce CO_2 emissions, which accounts in 2021 "for around 37% of energy- and process-related CO_2 emissions and over 34% of energy demand globally"[1]One of the straightforward ways to achieve such an objective is to extend the service life of the existing buildings and infrastructures. Extending the lifetime of large infrastructures such as long bridges and nuclear power plants would be beneficial not only for the reduction of CO_2 emissions but also from the economic point of view.

In 24 of the nuclear power plants in France, the confinement buildings are biaxially prestressed and do not have a metallic liner, which implies that airtightness is a matter for concrete alone. Prestressing is necessary to keep the airtightness of the buildings in case of an accident during which the internal pressure could increase up to 0.5 MPa[2]. It is well known that prestressing decreases over time, due to the relaxation of steel and to the delayed deformation of concrete. To ensure safety, these buildings are submitted to decennial verification of the prestress level and of the airtightness. If it is possible to predict correctly the evolution of the deformations of the containment vessel, it could be possible to extend their service time. In this case, the production of new reinforced and prestressed concretes and associated CO_2 emissions can be spared and savings will be achieved, considering the large size of the containment vessel: diameter ~40 m, height ~60 m and wall thickness ~ 1 m.

Our knowledge about the delayed deformations of concrete, i.e. creep and shrinkage, has been improved since the construction of the old nuclear power plants forty years ago. Currently, it is accepted that the delayed deformation is caused by the volumetric instability of calcium silicate hydrates (C-S-H), which is the main hydrate phase in Portland cement[3]. Although physical models[4–9], numerical simulations[10–12] and molecular dynamics[13,14] have been applied to understand and predict the long-term evolution of creep and shrinkage, experimental results and in-situ measurements are still necessary to verify the applicability. A comprehensive database of creep and shrinkage experiments was compiled at Northwestern University in the US[15]. Most of the experimental studies are limited to a short duration, i.e. several months to a few years due to the practical limitations in laboratory studies. The longest experiments were 12-year long uniaxial and biaxial creep tests performed at EDF[16], and 30-year long uniaxial creep and shrinkage experiments performed by Brooks[17]; long-term in-situ measurements are rare. To fill this gap, this paper aims to present in-situ strain measurements on four nuclear power plants for 30-40 years. Also, a simple but

practical method for predicting long-term delayed strain of concrete will be proposed.

In the following, we start with a brief presentation of four components of delayed strain and their prediction laws in the next generation Eurocode 2 (EC2) as well as the stress relaxation law of steel[18]. Then, laboratory experiments which characterize the delayed deformation behavior of the concrete of containment vessel in four nuclear power plants will be presented, followed by in-situ measurements of strains of these containment vessels. Finally, strains will be estimated for three sets of parameters in the EC2 relations and compared with the in-situ measurement.

2 Delayed strains of concrete in next-generation EC2

Concrete is a viscoelastic material, which means that when a concrete structure is subjected to a load lower than its elastic limit, there will be an instantaneous deformation at the time of loading, called elastic deformation ε^e and, a delayed deformation ε^{de}, which will evolve, even without a change in the applied load.

In recent models (such as[12]) or standards like the EC2[18] or the fib model code 2020 (MC2020)[19], the delayed strain ε^{de} of concrete is regarded as the sum of four decoupled components: autogenous shrinkage ε^{as}, drying shrinkage ε^{ds}, basic creep ε^{bc}, and drying creep ε^{dc}:

$$\varepsilon^{de} = \varepsilon^{as} + \varepsilon^{ds} + \varepsilon^{bc} + \varepsilon^{dc} \tag{1}$$

Autogenous shrinkage is the deformation of a load-free sealed concrete specimen, i.e. without any water exchange with its surrounding environment. The origin of autogenous shrinkage has been widely studied and many studies consider it as the deformation under the capillary forces which are caused by self-desiccation, for instance[20–26]. Recently, others studies suggested that the colloidal eigenstress of hydrates is the driving force of autogenous shrinkage[27]. Whether an asymptotic form of autogenous shrinkage evolution is also still under debate: In[23–25], autogenous shrinkage is modelled as an elastic strain hence with an asymptote, whereas as a logarithmic function of time, hence without asymptotic value, in other models [20,22,26,28,29]; in MC2020, autogenous shrinkage is modelled as a function of the compressive strength f_{cm} and cement type (Eq.(2)):

$$\varepsilon^{as} = \xi_{cbs1}\alpha_{as}\left(\frac{0.1\,f_{cm}}{6+0.1\,f_{cm}}\right)\left(1-e^{-0.2\xi_{cbs2}\sqrt{t}}\right) \tag{2}$$

where t is the age of concrete, α_{as} is a parameter depending on cement type, ξ_{cbs1}

and ξ_{cbs2} are fitting parameters for the magnitude of the final value and the kinetics, respectively. By default, the values of these two fitting parameters are equal to 1. However, it is possible to choose other values than 1 in the cases where material experiments are performed or in-situ measurements are available.

Drying shrinkage is defined as the deformation of a load-free drying specimen minus the autogenous shrinkage. Drying shrinkage is considered, in general, as the deformation caused by the internal forces due to the drying, though different opinions exist on the nature and contributions of the involving forces (for instance [8,28,29]): capillary forces, disjoining pressure. Some [28–33] consider drying shrinkage as an elastic deformation that reaches its asymptotic value when drying reaches its final state, whereas others [11,34–36] consider it as viscoelastic, implying that drying shrinkage has no asymptote. In design codes, drying shrinkage is modelled with an asymptote. In MC2020, the final drying shrinkage depends on the compressive strength f_{cm}, cement type, and relative humidity of the drying environment, while the kinetics also depend on the notional size of the element in addition to the other parameters.

$$\varepsilon^{ds} = \xi_{cds1}[(220 + 110\alpha_{ds1})e^{-\alpha_{ds2}f_{cm}}]\beta_{RH}\left[\frac{(t - t_s)}{0{,}035\xi_{cds2}h^2 + (t - t_s)}\right]^{0.5} \quad (3)$$

Where t_s is the age of concrete when drying starts, h is the notional size of the concrete element, α_{ds1} and α_{ds2} are parameters that depend on cement class, β_{RH} is a function of relative humidity specified in MC2010, ξ_{cds1} and ξ_{cds2} are fitting parameters for the magnitude of the final value and the kinetics of drying shrinkage, respectively. Similarly to the case of autogenous shrinkage, these two parameters are allowed to be adjusted.

Basic creep is defined as the difference between the deformation of a loaded sealed specimen and the autogenous shrinkage. It is believed that basic creep originates from the main hydrate C-S-H while the physical mechanism is not yet fully understood. Several theories exist to explain the mechanism of creep for load levels lower than 40% of the strength: microprestress theory,[37,38] local macroscopic relaxation,[39] and dissolution-precipitation phenomenon[40]. The majority of researches and design codes consider that basic creep evolves as a function of time with a non asymptotic value in the long term. In MC2020, basic creep is a function of the concrete strength and cement type:

$$\varphi_{bc}(t,t_0) = \xi_{bc1}\frac{1.8}{(f_{cm})^{0.7}} ln\left(1 + (\frac{30}{t_{0,adj}} + 0.035)^2 \frac{(t-t_0)}{\xi_{bc2}}\right) \quad (4)$$

where φ_{bc} is the basic creep coefficient, defined as the ratio of creep strain over elastic strain due to the same load σ_0, i.e. $\varepsilon^{bc} = \varphi_{bc}\sigma_0/E_c$ with E_c as the modulus of elasticity of concrete; t_0 and $t_{0,adj}$ are the age of loading and the adjusted age of loading accounting for the curing temperature; ξ_{bc1} and ξ_{bc2} are fitting parameters for the magnitude of the final value and the kinetics of basic creep, respectively. Similar to the case of autogenous shrinkage, these two parameters are allowed to be adjusted.

Drying creep is the least studied type of delayed strain. When a loaded specimen is subjected to drying, the delayed deformation is larger than the sum of autogenous shrinkage, drying shrinkage, and basic creep. This supplementary deformation part is defined as drying creep. As for the origin, in line with the microprestress theory of basic creep, the drying creep was explained by an amplified delayed strain due to the water movement[41–43]. In contrast, Sellier et al. explained that the mechanical consequences of capillary forces are enforced in the presence of load hence causing a supplementary drying shrinkage part corresponding to drying creep[11]. MC2020 specifies the drying creep coefficient φ_{dc} is defined as the ratio of drying creep strain ε^{dc} over elastic strain due to the same load σ_0, i.e. $\varepsilon^{dc} = \varphi_{bc}\sigma_0/E_c$. In MC2020, the drying creep coefficient is a function of concrete strength, cement type, age of loading, and ambient relative humidity and is given by the following expression:

$$\varphi_{dc}(t,t_0) = \xi_{dc1}\frac{412}{(f_{cm})^{1.4}}\frac{1-\frac{RH}{100}}{\sqrt[3]{0.1\frac{h}{100}}}\frac{1}{0.1+(t_{0,adj})^{0.2}}\left[\frac{t-t_0}{\xi_{dc2}\beta_h + t - t_0}\right]^{\gamma(t_0)} \quad (5)$$

where *RH* is the relative humidity of the environment, *h* is the notional size, β_h is a parameter to account for the impact of strength and notional size on the kinetics, $\gamma(t_0)$ is a parameter to account for the impact of loading age t_0 on the kinetics; ξ_{dc1} and ξ_{dc1} are fitting parameters for the magnitude of the final value and the kinetics of basic creep, respectively. Similarly, these two parameters are allowed to be adjusted.

The equations 2 to 5 are given for a reference temperature of 20 °C. Higher temperature accelerates the kinetics of creep and shrinkage strains. For basic creep, the influence of temperature can be considered by a thermo-activation term on the kinetics [44]: in Eq.(4), the term in the denominator ξ_{bc2} is multiplied by an Arrhenius-type activation term $\exp\big(Q(1/T - 1/T_0)\big)$, in which $Q = 6000$ K^{-1} is the

activation energy, T and T_0 are the actual and reference temperatures, in K. For drying creep, the influence of temperature is considered following the proposition of MC2020. On one hand, temperature influences kinetics: the term $\xi_{dc2}\beta_h$ is multiplied by an Arrhenius-type activation term $\beta_T = \exp(1500/T - 5.12)$, with T actual temperature in K; On the other hand, the amplitude of drying creep is also multiplied by $\left(\exp\left(0.015(T-20)\right)\right)^2$, with T actual temperature in °C.

All these previous equations are used to estimate the delayed strains at the material scale since they are based on laboratory datas. Nevertheless, they are expected to predict an average strain on the cross-section of concrete elements. In the following, we will use these equations to estimate the average delayed strains of containment vessels.

3 Stress relaxation of steel

Under the condition of constant strain, the stress in the steel will relax over time. As proposed in MC2020, the kinetics of stress relaxation in steel is described by the time evolution of prestress loss:

$$\rho(t) = \rho_{1000}\left(\frac{t}{1000}\right)^k \quad (6)$$

with $\rho(t)$ is the prestress loss, defined as $\rho(t) = (\sigma_0 - \sigma(t))/\sigma_0$; t is the time since the application of the prestress by a strain ε_0 that will be kept constant. σ_0 and $\sigma(t)$ are the stress at the time of application of ε_0 and at time t, respectively; $k = \log(\rho_{1000}/\rho_{100})$; ρ_{100} and ρ_{1000} are the prestress loss at 100 hours and 1000 hours, respectively.

The Equation 6 is given for a reference temperature of 20 °C. For other temperatures, the stress loss rate should be multiplied by a factor $\alpha_T = T/20$, with T actual temperature in °C.

4 Data from laboratory experiments and in-situ measurement

This section presents experimental data related to delayed strain of containment vessels in four nuclear power plants (NPPs), named hereafter A, B, C, D for the sake of confidentiality. These containment vessels were designed 50 years ago based on the requirement for strength, and delayed deformations were estimated with relations used at this period. A decade later, when the first concerns arose about the delayed

deformations of certain containment vessels, experimental studies were performed on concrete with the same mixtures[45]. In the following, there laboratory experiments will be presented, follows then characteristics of the containment vessel and results of in-situ measurement.

4.1 Material characterization in the laboratory

To characterize the delayed deformation behaviour of the the four power plants A-D, cylindrical specimens 1 m high and 16 cm in diameter were prepared by Granger[45]. Following the experimental method proposed in LCPC[46], these specimens were cured for 28 days at 20°C under sealed conditions. At the age of 28 days, the specimens were instrumented in the vertical direction with a displacement meter. To avoid errors due to boundary conditions, the length change was measured only in the central part of the specimen over a height of 30 cm.

Four types of tests were performed at a temperature of 20°C:

- Sealed load-free specimen: the length change of the specimen was used to obtain the autogenous shrinkage (see Figure 1a).
- Drying load-free specimen: the relative humidity of the test room was 50%. Drying shrinkage was obtained by subtracting the autogenous shrinkage from the measured shrinkage strain of the specimen (see Figure 1b).

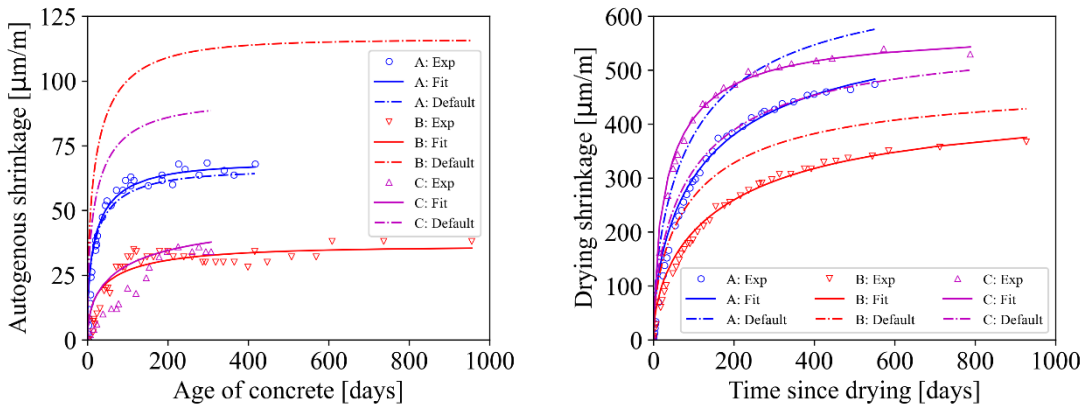

(a) (b)

Figure 1 Autogenous and drying shrinkage of specimens. Default corresponds to the use of default values of parameters in equations 2 and 3. Fit corresponds to the use of fitted values in equations 2 and 3.

- Sealed loaded specimen: a uniaxial load of 13 MPa was applied with a hydraulic

pressure tank and kept constant during the whole duration of the test. Subtracting the autogenous shrinkage from the measured strain, the basic creep strain was obtained (Figure 2a).

- Drying loaded specimen: a uniaxial load of 13 MPa was applied with a hydraulic pressure tank and kept constant during the whole duration of the test. The relative humidity of the room was 50%. Subtracting the sum of autogenous shrinkage, drying shrinkage and basic creep from the measured strain, the drying creep strain was obtained (Figure 2b).

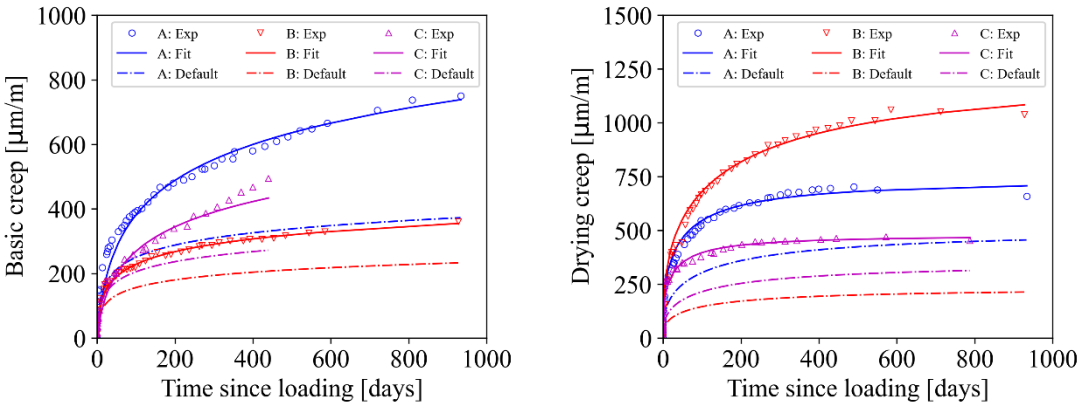

(a) (b)

Figure 2 Basic creep and drying creep of specimens. Default corresponds to the use of default values of parameters in equations 2 to 5. Fit corresponds to the use of fitted values in equations 2 to 5.

The experimental results are compared with the default laws described in Eqs.2-5, considering two different cases. Firstly, knowing the mixture design, compressive strength, and size of the specimens, we computed the time evolution of the four components of the delayed strain by taking all the fitting parameter as 1. These default predictions were plotted with dash-dot lines in Figure 1 and Figure 2 and compared with the measured results. The default predictions deviate significantly from the experimental results.

Then, using a least square optimization method, the experimental results were fitted against Eqs.2-5 by adjusting the fitting parameters. The target was to reduce the weighted sum of the squares of the residuals (i.e. the difference between an experimental value and the value computed from MC2020 equations). The weight for the sum was proportional to time, giving more importance to long-term values. The set

of values of fitting parameters that gives the least weighted sum of the squares of the residual was taken as the results and summarized in Table 1. A larger deviation from 1 means a larger gap between the default law and the experimental results.

Table 1 Fitting parameters of delayed strain laws: default and best fit.

Delayed strain		Autogenous shrinkage		Drying shrinkage		Basic creep		Drying creep	
Parameters		ξ_{cbs1}	ξ_{cbs2}	ξ_{cds1}	ξ_{cds2}	ξ_{bc1}	ξ_{bc2}	ξ_{dc1}	ξ_{dc2}
Default		1	1	1	1	1	1	1	1
Best fit	A	1	1	0.9	1.3	5	5	1.5	0.4
	B	0.3	0.7	0.9	1.8	1.7	1.7	5.3	1.6
	C&D	0.5	0.5	1	0.4	2.6	10	1.3	0.2

4.2 Instrumented confinement buildings in four nuclear power plants

The containment vessel of the four NPPs is a biaxially prestressed concrete structure, constructed some forty years ago with ordinary Portland cement concrete. The designed strength, Young's modulus and mixture proportion are listed in Table 2. Note that the same concrete was used for the C and D vessels.

Table 2 Mixture proportion, strength and Young's modulus of the concrete, wall thickness, age of prestressing and service of the confinement buildings.

Powerplant	Compressive strength [MPa]	Young's modulus [GPa]	Cement class	Cement strength	Wall thickness [mm]	Age at prestress [days]	Age at service [days]
A	42	31	R	52.5 N	1200	769	2632
B	64.5	36.7	R	52.5 N	1200	735	2571
C	53.4	31.9	R	52.5 N	900	426	1552

D	53.4	31.9	R	52.5 N	900	452	1461

The concrete was prestressed with vertical and horizontal (hoop) tendons. The vertical tendons were prestressed in several steps, lasting for almost two years. However, for the sake of simplicity, it was assumed here to be applied instantaneously, at the same time as horizontal prestress. The stress level and section of tendons in vertical and horizontal directions are summarized in Table 3.

Table 3 Prestress values and section of prestressing tendons.

	Vertical prestress [MPa]	Horizontal prestress [MPa]	Vertical tendon [m^2/m^2-concrete]	Horizontal tendon [m^2/m^2-concrete]
A & B	8.53	12.53	0.0056	0.0128
C & D	9.45	13.02	0.0068	0.0143

The strain and temperature in the containment vessels were measured at the mid-height of the building with embedded sensors, placed far away from unusual features such as the hatch. In the containment vessels of A and B, there were two strain sensors, located 15 cm away from the external and internal surfaces, respectively. In the containment vessels of C and D, there were also two strain sensors, 10 cm away from the external and internal surfaces, respectively. The evolutions of the strain over time by these sensors are displayed in Figure 4, Figure 5, and Figure 6.

5 Prediction of delayed strain accounting in-situ temperature history

The objective of the section is to model the delayed strains of the four confinement buildings using the delayed strain laws Eqs.2-5. Assuming plane sections to be able to have an analytical modelling (i.e. without the use of a finite element modelling), we consider a material point of concrete which is submitted to vertical stress and horizontal stress to predict the strain evolution over time.

The simulation methodology is the same as the one proposed in [47]. Here, we present only the main lines. Given the varying stress due to stress relaxation, the superposition principle was used. The superposition principle can be applied either by decomposing the stress history horizontally into stress increments, or by vertically into stress pulses. Only vertical decomposition can be used when the influence of a varying temperature has to be considered[48].

In this study, we consider the effect of varying temperature on the basic and drying creep strains, hence the total time length was divided into n steps with a step length of 1 day while stress history is decomposed into n vertical pulses. For the calculation of each step, temperature and stress are considered to be constant. Each of the n steps consists of four substeps:

Substep 1: the incremental strain of concrete was calculated in both directions, by summing up the elastic strain, and the four components of delayed strain. For instance at step i in the vertical direction, the strain $\varepsilon_{i+1}^{c,ve}$ computes as:

$$\varepsilon_{i+1}^{c,v} = \frac{\sigma_i^{c,v} - \nu\sigma_i^{c,h}}{E_c} + \varepsilon_{i+1}^{bc,v} + \varepsilon_{i+1}^{dc,v} + \varepsilon_{i+1}^{ds} + \varepsilon_{i+1}^{as} \tag{8}$$

where E_c and ν are the elastic modulus (values taken from Table 2) and elastic Poisson's ratio of concrete, which is taken to be equal to 0.2 based on literature data gathered in [49]; $\sigma_i^{c,v}$ and $\sigma_i^{c,h}$ are the vertical and horizontal stress pulses at step i, obtained in the previous step; ε_{i+1}^{as}, ε_{i+1}^{ds}, $\varepsilon_{i+1}^{bc,v}$ and $\varepsilon_{i+1}^{dc,v}$ are, respectively, the autogenous shrinkage, drying shrinkage, vertical basic creep and vertical drying creep at the step i. Among them, autogenous shrinkage ε_{i+1}^{as} is computed using Eq. (2); Drying shrinkage is computed using Eq. (3) while taking into account the impact of varying relative humidity by the concept of equivalent time [47]. It is well known that drying shrinkage is accelerated with the increase of temperature and such impact of temperature can be considered with the relations proposed in MC2020. However, such a method is limited to isothermal conditions. Given the difficulty of accounting for the impact of a varying temperature on drying shrinkage, temperature was not considered in this simplified study. Basic creep and drying creep are calculated with the superposition principle, considering the sum of the response of all the stress pulses until the current step. Stress pulse at step j is equivalent to a combination of the following two: loading $\left(\sigma_j^{c,v}, \sigma_j^{c,h}\right)$ at time t_j of the beginning of the step j, and unloading $\left(\sigma_j^{c,v}, \sigma_j^{c,h}\right)$ at time $t_j + dt_j$ of the end of the step j. For instance, the calculation of basic creep in the vertical direction reads as:

$$\begin{aligned}\varepsilon_{i+1}^{bc} = {} & \left(\sigma_i^{c,v} - \nu_b\sigma_i^{c,h}\right) \cdot \frac{\left(\varphi_{bc}(t_{i+1}, t_i, T(t_i)\right)}{E_c} \\ & + \sum_{j=0}^{i-1} \left(\sigma_j^{c,v} - \nu_b\sigma_j^{c,h}\right) \frac{\left(\varphi_{bc}\left(t_{i+1}, t_j, T(t_j)\right) - \varphi_{bc}\left(t_{i+1}, t_j + dt_j, T(t_j)\right)\right)}{E_c}\end{aligned} \tag{9}$$

where ν_b is the Poisson's ratio of basic creep, $T(t_i)$ is the temperature at time t_i obtained from a simplified temperature history (see Figure 3) based on measurement. The value of ν_b is taken to be equal to 0.2 and independent of time, based on gathered data in [49].

For the drying creep, it is sufficient to replace φ_{bc} and ν_b in Eq.(9) by φ_{dc} and ν_d, respectively. The drying creep Poisson's ratio ν_d is considered to be 0 as proposed in a previous work[47] meaning that drying creep in one direction does not induce creep in the perpendicular direction. Note that a value equal to the elastic Poisson ratio is also possible[50] inducing only a small difference in the results[47] .

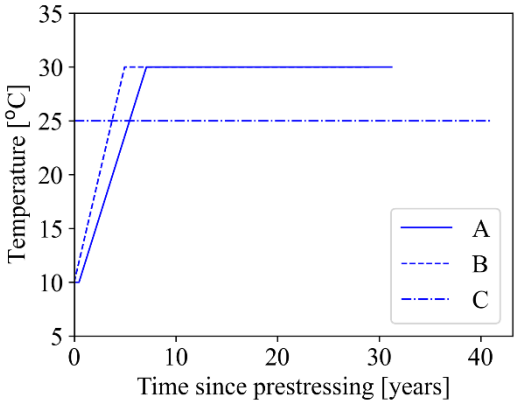

Figure 3 Simplified temperature history based on in-situ measurement.

Substep 2: considering the continuity of displacement, the same incremental strains were added to vertical and horizontal tendons. For vertical direction, this reads as:

$$\varepsilon_{i+1}^{s,v} = \varepsilon_i^{s,v} + \left(\varepsilon_{i+1}^{c,v} - \varepsilon_i^{c,v}\right) \tag{10}$$

where $\varepsilon_i^{s,v}$ represents the strain in the vertical steel tendons at step i. The strain in horizontal tendons is also updated in the same way.

Substep 3: stresses in tendons were calculated considering steel relaxation at each time step. Since the strains in tendons are not constant, the superposition principle is applied in the same manner as Eq.(9). Strain history is decomposed vertically into strain pulses hence the stress loss at step i is a consequence of relaxation due to all previous strain pulses. For instance, the calculation of stress in the vertical tendons reads as:

$$\sigma_{i+1}^{s,v} = E_s \varepsilon_{i+1}^{s,v}\left(1 - \alpha_T(T_i)\rho(t_{i+1}, t_i)\right) + \sum_{j=0}^{i-1} E_s \varepsilon_j^{s,v}\left(\left(1 - \alpha_T(T_j)\rho(t_{i+1}, t_j)\right) - \left(1 - \alpha_T(T_j)\rho(t_{i+1}, t_j + dt_j)\right)\right) \quad (11)$$

where $\sigma_i^{s,v}$ represents stress in the vertical steel tendons at step i, and E_s is the elastic modulus of the tendons, taken to be equal to 190 GPa.

Substep 4: stresses in concrete were calculated from the equilibrium of forces. For instance, the stress in the vertical direction is computed by

$$\sigma_{i+1}^{c,v} = \sigma_{i+1}^{s,v} \frac{A_{s,v}}{A_{c,v}} \quad (12)$$

where $\sigma_i^{c,v}$ represents vertical stress in concrete at step i, and $A_{s,v}/A_{c,v}$ is the section of vertical tendon per concrete section, summarized in Table 3. Horizontal stress in concrete is also calculated in the same way.

The simulations were performed with three sets of delayed strain laws which are listed in Table 1: i) default value; ii) fitted values that give the best fit of laboratory experiments; iii) characteristic fitted values obtained with statistical analysis of in-situ measurement on 17 containment vessels including the 4 containments that are considered in section 4[51].

The last set of parameters were fitted on the measurements of tangential and vertical strains of real containments with the following assumptions:

- Autogenous shrinkage was neglected (because prestressing was applied at an age older than 6 months),

- Basic creep parameters (equation 4) were fitted on the difference between vertical and tangential strains,

- Drying creep and drying shrinkage parameters (equations 3 and 5) were fitted on the average between vertical and tangential strains. This assumption corresponds to a drying creep Poisson ratio equal to 0.

The amplitudes of shrinkage and creep obtained with these fitted values were compared with amplitudes obtained from MC2020. A distribution of the ratio between real and predicted with default values was obtained for creep and for shrinkage. The fractile at 95% of the distribution is equal to 1.9 for creep and 1.7 for shrinkage. For the comparison, the parameters affecting kinetics are kept as default values, i.e. 1. Note

that, with these characteristic values of the parameters, predicted delayed strains will be generally larger than the observed strains.

Modelling results are displayed in Figure 4 to Figure 6. For vertical strains a larger variability is observed in the measurements. This could not be explained by the mechanical behavior (plane sections) but may be due to a position error affecting the measurement by the extensometers. The initial value of the measured strain was different from the one calculated using the modulus of elasticity. To observe the delayed part of the strain, the calculated strain was shifted so that the initial values overlap the measurement.

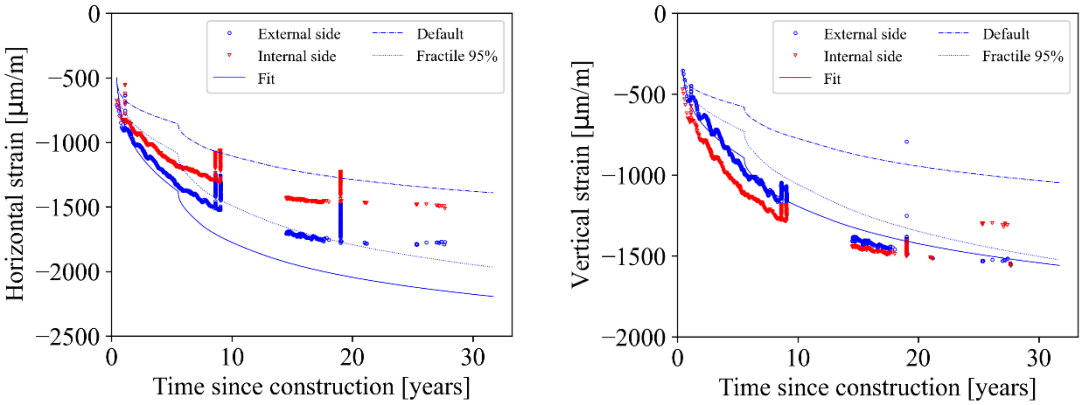

(a) (b)

Figure 4 Measured and calculated strains of containment vessel A

Simulations with default parameters underestimate the delayed strains of concrete, for all of the four containment vessels. The estimated delayed strains with best-fit parameters are larger than the ones with fractile 95% in case A and very close in case B. For C and D cases, predictions with fitted parameters corresponding to the fractile 95% give higher delayed strains. When the increasing rates of delayed strains are compared, modelling with parameters of fractile 95% predicts the faster increase rates.

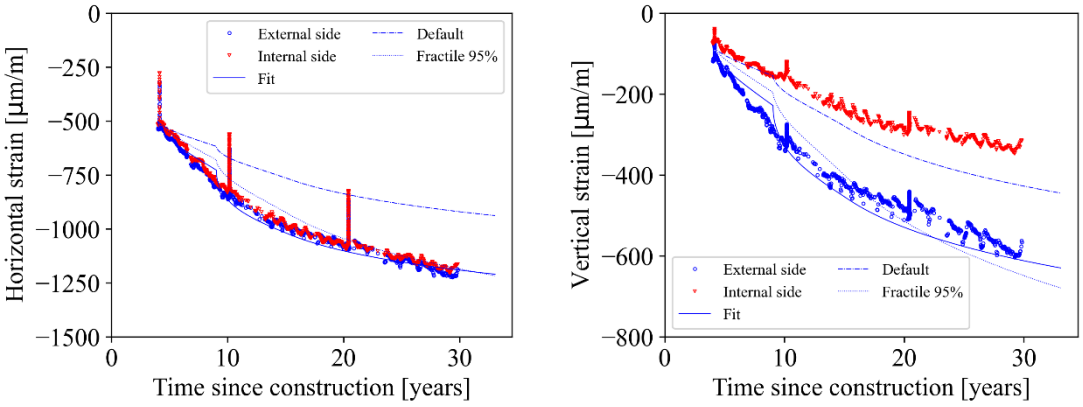

(a) (b)

Figure 5 Measured and calculated strains of the containment vessel B

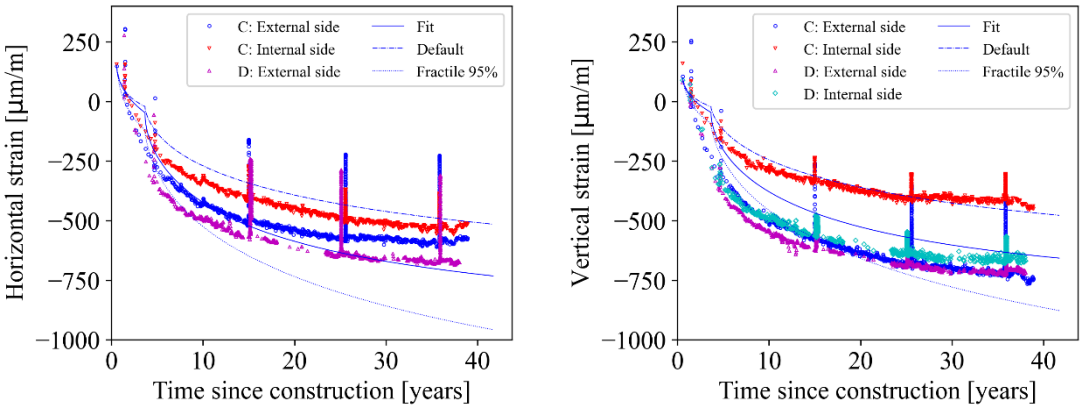

(a) (b)

Figure 6 Measured and calculated strains of the containment vessels C and D

Despite the simplicity of representing the whole containment vessel by a single material point, the results of the simulation with the best fitting parameters agree reasonably well with the in-situ measurement. Among the three simulations, the use of the default values deviates most from the real measurements. In engineering practice, it would be better if creep and shrinkage tests could be performed to obtain the best-fitting parameters. However, these tests are time-consuming and require sophisticated laboratory conditions. Therefore, establishing a database of in-situ measurement and providing values for fitting parameters corresponding to fractiles 95% could be a more efficient and beneficial way.

6 Conclusion

We presented 30-year in-situ strain measurements on the containment vessel of four nuclear power plants. Based on the laboratory experiments characterizing the concrete of these confinement buildings, we predicted the delayed strain using the evolution law of shrinkage and creep in the next generation EC2. The following conclusions are:

- Delayed strains of concrete continue increasing even 30 years after construction.
- Default laws given in Eurocode 2 underestimate the delayed strain for the examples of this paper. A statistical analysis of in-situ measurements on 17 nuclear power plants, has shown that, for a 95% fractile value, the fitting parameter for the shrinkage magnitude is equal to 1.7, and for the creep magnitude 1.9. These values could be lower in the case of recent nuclear power plants where high-performance concretes were used.
- The proposed method considering shrinkage, biaxial creep and steel relaxation with the effect of temperature on these phenomena can adapt the constitutive relations if delayed strains of concrete are characterized by laboratory experiments.
- Modelling at material scale with the adjusted parameters predicts delayed strains of concrete in reasonable agreement with in-situ measurements.

Delayed strains of concrete depend on many parameters in addition to the strength. As the variety of cementitious materials increases, especially in the context of low carbon concretes, the method presented in this study is particularly useful: the method provides the possibility to fit material parameters with laboratory experiments.

Reference

1. United Nations Environment Program. 2022 Global Status Report for Buildings and Construction. Published online 2022.
2. Charpin L, Niepceron J, Corbin M, et al. Ageing and air leakage assessment of a nuclear reactor containment mock-up: VERCORS 2nd benchmark. *Nuclear Engineering and Design*. 2021;377(March). doi:10.1016/j.nucengdes.2021.111136
3. Mehta PK, Monteiro PJM. *Concrete: Microstructure, Properties, and Materials*. 3rd ed. McGraw-Hill New York; 2006.

4. Vandamme M. Two models based on local microscopic relaxations to explain long-term basic creep of concrete. *Proceedings of the Royal Society A: Mathematical, Physical and Engineering Sciences*. 2018;474(2220). doi:10.1098/rspa.2018.0477

5. Pignatelli I, Kumar A, Alizadeh R, Le Pape Y, Bauchy M, Sant G. A dissolution-precipitation mechanism is at the origin of concrete creep in moist environments. *Journal of Chemical Physics*. 2016;145(5). doi:10.1063/1.4955429

6. Bazant ZP, Hauggaard AB, Baweja S, Ulm F josef. Creep . I : Aging and Drying Effects. *J Eng Mech*. 1997;123(Pickett 1942):1188-1194.

7. Rahimi-Aghdam S, Bažant ZP, Cusatis G. Extended Microprestress-Solidification Theory for Long-Term Creep with Diffusion Size Effect in Concrete at Variable Environment. *J Eng Mech*. 2019;145(2):1-14. doi:10.1061/(asce)em.1943-7889.0001559

8. Nguyen H, Rahimi-Aghdam S, Bažant ZP. Unsaturated nanoporomechanics. *Proceedings of the National Academy of Sciences*. 2020;117(7):3440-3445.

9. Aili A, Vandamme M, Torrenti JM, Masson B. A viscoelastic poromechanical model for shrinkage and creep of concrete. *Cem Concr Res*. 2020;129(June 2019):105970. doi:10.1016/j.cemconres.2019.105970

10. Benboudjema F, Meftah F, Torrenti JM. A viscoelastic approach for the assessment of the drying shrinkage behaviour of cementitious materials. *Mater Struct*. 2007;40(2):163-174.

11. Sellier A, Multon S, Buffo-Lacarrière L, Vidal T, Bourbon X, Camps G. Concrete creep modelling for structural applications: non-linearity, multi-axiality, hydration, temperature and drying effects. *Cem Concr Res*. 2016;79:301-315.

12. Wendner R, Hubler MH, Bažant ZP. The B4 Model for Multi-decade Creep and Shrinkage Prediction. In: *Mechanics and Physics of Creep, Shrinkage, and Durability of Concrete*. ; 2013:429-436. doi:10.1061/9780784413111.051

13. Masoumi S, Valipour H, Abdolhosseini Qomi MJ. Interparticle Interactions in Colloidal Systems: Toward a Comprehensive Mesoscale Model. *ACS*

Appl Mater Interfaces. 2017;9(32):27338-27349. doi:10.1021/acsami.7b08465

14. Morshedifard A, Masoumi S, Abdolhosseini Qomi MJ. Nanoscale origins of creep in calcium silicate hydrates. *Nat Commun*. 2018;9(1). doi:10.1038/s41467-018-04174-z

15. Hubler MH, Wendner R, Bažant ZP. Comprehensive Database for Concrete Creep and Shrinkage: Analysis and Recommendations for Testing and Recording. *ACI Mater J*. 2015;112(4). doi:10.14359/51687453

16. Charpin L, Pape Y Le, Coustabeau É, et al. A 12year EDF study of concrete creep under uniaxial and biaxial loading. *Cem Concr Res*. 2018;103:140-159. doi:https://doi.org/10.1016/j.cemconres.2017.10.009

17. Brooks JJ. 30-year creep and shrinkage of concrete. *Magazine of Concrete Research*. 2005;57(9):545-556.

18. CEN FprEN 1992-1-1. Eurocode 2: Design of concrete structures—Part 1-1: General rules,rules for buildings, bridges and civil engineering structures. *Brussels: CEN*. Published online April 2023.

19. Fib model code 2020. *Fib Model Code for Concrete Structures 2020*. final draft.; 2023.

20. Hua C, Acker P, Ehrlacher A. Analyses and models of the autogenous shrinkage of hardening cement paste. I. Modelling at macroscopic scale. *Cem Concr Res*. 1995;25(7):1457-1468. doi:10.1016/0008-8846(95)00140-8

21. Ulm FJ, Le Maou F, Boulay C. Creep and shrinkage coupling : New review of some evidence. *Revue Française de Génie Civil*. 1999;3:21-37.

22. Wyrzykowski M, Lura P, Pesavento F, Gawin D. Modeling of internal curing in maturing mortar. *Cem Concr Res*. 2011;41(12):1349-1356. doi:10.1016/j.cemconres.2011.04.013

23. Zhang J, Hou D, Han Y. Micromechanical modeling on autogenous and drying shrinkages of concrete. *Constr Build Mater*. 2012;29:230-240.

24. Lin F, Meyer C. Modeling shrinkage of portland cement paste. *ACI Mater J*. 2008;105(3):302-311.

25. Lura P, Jensen OM, van Breugel K. Autogenous shrinkage in high-performance cement paste: an evaluation of basic mechanisms. *Cem Concr Res*. 2003;33(2):223-232.

26. Aili A, Vandamme M, Torrenti JM, Masson B. Is long-term autogenous shrinkage a creep phenomenon induced by capillary effects due to self-desiccation? *Cem Concr Res*. 2018;108:186-200.

27. Abuhaikal M, Ioannidou K, Petersen T, Pellenq RJM, Ulm FJ. Le Châtelier's conjecture: Measurement of colloidal eigenstresses in chemically reactive materials. *J Mech Phys Solids*. 2018;112:334-344. doi:10.1016/j.jmps.2017.12.012

28. El Tabbal G, Dangla P, Vandamme M, Bottoni M, Granet S. Modelling the drying shrinkage of porous materials by considering both capillary and adsorption effects. *J Mech Phys Solids*. Published online 2020:104016.

29. Maruyama I. Origin of drying shrinkage of hardened cement paste: hydration pressure. *Journal of Advanced Concrete Technology*. 2010;8(2):187-200.

30. Gawin D, Pesavento F, Schrefler BA. Hygro-thermo-chemo-mechanical modelling of concrete at early ages and beyond. Part II: shrinkage and creep of concrete. *Int J Numer Methods Eng*. 2006;67(3):332-363.

31. Coussy O. *Poromechanics*. John Wiley & Sons; 2004.

32. Di Bella C, Wyrzykowski M, Lura P. Evaluation of the ultimate drying shrinkage of cement-based mortars with poroelastic models. *Materials and Structures/Materiaux et Constructions*. 2017;50(1):1-13. doi:10.1617/s11527-016-0870-0

33. Allen AJ, Fagerlund G, Scrivener KL, et al. Hysteresis from multiscale porosity: modeling water sorption and shrinkage in cement paste. *Cem Concr Res*. 2019;6(3):31-43. doi:10.1016/j.conbuildmat.2011.07.017

34. Grasley ZC, Leung CK. Desiccation shrinkage of cementitious materials as an aging, poroviscoelastic response. *Cem Concr Res*. 2011;41(1):77-89. doi:10.1016/j.cemconres.2010.09.008

35. Rahimi-Aghdam S, Masoero E, Rasoolinejad M, Bažant ZP. Century-long

expansion of hydrating cement counteracting concrete shrinkage due to humidity drop from selfdesiccation or external drying. *Mater Struct*. 2019;52(1):11.

36. Aili A, Vandamme M, Torrenti JM, Masson B. A viscoelastic poromechanical model for shrinkage and creep of concrete. *Cem Concr Res*. 2020;129:105970.

37. Bažant ZP, Hauggaard AB, Baweja S, Ulm F josef. Microprestress-Solidification Theory for Concrete Creep. I: Aging and Drying Effects. *J Eng Mech*. 1997;123(11):1188-1194. doi:10.1061/(ASCE)0733-9399(1997)123:11(1188)

38. Rahimi-Aghdam S, Bažant ZP, Cusatis G. Extended microprestress-solidification theory for long-term creep with diffusion size effect in concrete at variable environment. *J Eng Mech*. 2019;145(2):04018131. doi:10.1061/(ASCE)EM.1943-7889.0001559

39. Vandamme M. Two models based on local microscopic relaxations to explain long-term basic creep of concrete. *Proceedings of the Royal Society A: Mathematical, Physical and Engineering Sciences*. 2018;474(2220). doi:10.1098/rspa.2018.0477

40. Pignatelli I, Kumar A, Alizadeh R, Le Pape Y, Bauchy M, Sant G. A dissolution-precipitation mechanism is at the origin of concrete creep in moist environments. *Journal of Chemical Physics*. 2016;145(5). doi:10.1063/1.4955429

41. Bazant ZP, J. C. Chern. Concrete creep at variable humidity: constitutive law and mechanism. *Mater Struct*. 1985;18(103):1-20.

42. Vlahinić I, Thomas JJ, Jennings HM, Andrade JE. Transient creep effects and the lubricating power of water in materials ranging from paper to concrete and Kevlar. *J Mech Phys Solids*. 2012;60(7):1350-1362. doi:10.1016/j.jmps.2012.03.003

43. Sinko R, Vandamme M, Bažant ZP, Keten S. Transient effects of drying creep in nanoporous solids: understanding the effects of nanoscale energy barriers. *Proceedings of the Royal Society A: Mathematical, Physical and Engineering Sciences*. 2016;472(2191):20160490.

doi:10.1098/rspa.2016.0490

44. Frech-Baronet J, Sorelli L, Chen Z. A closer look at the temperature effect on basic creep of cement pastes by microindentation. *Constr Build Mater*. 2020;258:119455. doi:10.1016/j.conbuildmat.2020.119455

45. Granger L. *Comportement Différé Du Béton Dans Les Enceintes de Centrales Nucléaires: Analyse et Modélisation*. Ecole Nationale des Ponts et Chaussées; 1995.

46. Acker P, Agullo L, Auperin M, et al. Standardized Test Methods for Creep and Shrinkage. *Mater Struct*. 1998;31:507-512.

47. Aili A, Torrenti JM. Modeling long-term delayed strains of prestressed concrete with real temperature and relative humidity history. *Journal of Advanced Concrete Technology*. 2020;18(7):396-408. doi:10.3151/jact.18.396

48. Walraven JC, Shen JH. On the Applicability of the Superposition Principle in Concrete Creep. *Mechanics of Creep Brittle Materials 2*. Published online 1991:282-295.

49. Aili A, Vandamme M, Torrenti JM, Masson B, Sanahuja J. Time evolutions of non-aging viscoelastic Poisson's ratio of concrete and implications for creep of C-S-H. *Cem Concr Res*. 2016;90:144-161. doi:http://dx.doi.org/10.1016/j.cemconres.2016.09.014

50. Charpin L, Sow TO, de Pradel XD, Hamon F, Mathieu JP. Numerical Simulation of 12 Years Long Biaxial Creep Tests: Efficiency of Assuming a Constant Poisson's Ratio. In: *Biot Conference on Poromechanics VI*. ; 2017:997-1004.

51. Barré F, Caba L, Torrenti JM, Aili A. Comparative study of the prediction of delayed strains using the next-generation Eurocode2 with measurements on structures - Application to the case of nuclear power plant containments, in: *conferenceTINCE'23, Technological Innovations in Nuclear Civil Engineering*, Saclay, France, 2023.